Acta Pharmaceutica Sinica B 2024;14(2):623−634

Chinese Pharmaceutical Association
Institute of Materia Medica, Chinese Academy of Medical Sciences

Acta Pharmaceutica Sinica B

www.elsevier.com/locate/apsb
www.sciencedirect.com

TOOLS

Transfer learning enhanced graph neural network for aldehyde oxidase metabolism prediction and its experimental application

Jiacheng Xiong[a,b,†], Rongrong Cui[a,b,†], Zhaojun Li[c,d,†], Wei Zhang[a,b], Runze Zhang[a,b], Zunyun Fu[a,b], Xiaohong Liu[d], Zhenghao Li[e], Kaixian Chen[a,b], Mingyue Zheng[a,b,f,*]

[a]*Drug Discovery and Design Center, State Key Laboratory of Drug Research, Shanghai Institute of Materia Medica, Chinese Academy of Sciences, Shanghai 201203, China*
[b]*University of Chinese Academy of Sciences, Beijing 100049, China*
[c]*College of Computer and Information Engineering, Dezhou University, Dezhou 253023, China*
[d]*AI Department, Suzhou Alphama Biotechnology Co., Ltd., Suzhou 215000, China*
[e]*Shanghai Institute for Advanced Immunochemical Studies, and School of Life Science and Technology, ShanghaiTech University, Shanghai 200031, China*
[f]*State Key Laboratory of Pharmaceutical Biotechnology, Nanjing University, Nanjing 210023, China*

Received 2 July 2023; received in revised form 7 September 2023; accepted 11 October 2023

KEY WORDS

Drug metabolism;
Aldehyde oxidase;
Transfer learning;
Graph neural network;
Kinase inhibitor

Abstract Aldehyde oxidase (AOX) is a molybdoenzyme that is primarily expressed in the liver and is involved in the metabolism of drugs and other xenobiotics. AOX-mediated metabolism can result in unexpected outcomes, such as the production of toxic metabolites and high metabolic clearance, which can lead to the clinical failure of novel therapeutic agents. Computational models can assist medicinal chemists in rapidly evaluating the AOX metabolic risk of compounds during the early phases of drug discovery and provide valuable clues for manipulating AOX-mediated metabolism liability. In this study, we developed a novel graph neural network called AOMP for predicting AOX-mediated metabolism. AOMP integrated the tasks of metabolic substrate/non-substrate classification and metabolic site prediction, while utilizing transfer learning from ^{13}C nuclear magnetic resonance data to enhance its performance on both tasks. AOMP significantly outperformed the benchmark methods in both cross-validation and external testing. Using AOMP, we systematically assessed the AOX-mediated metabolism of common fragments in kinase inhibitors and successfully identified four new scaffolds with AOX metabolism liability, which were validated through *in vitro* experiments. Furthermore, for the convenience of the community, we

*Corresponding author.
E-mail address: myzheng@simm.ac.cn (Mingyue Zheng).
†These authors made equal contributions to this work.
Peer review under the responsibility of Chinese Pharmaceutical Association and Institute of Materia Medica, Chinese Academy of Medical Sciences.

https://doi.org/10.1016/j.apsb.2023.10.008

established the first online service for AOX metabolism prediction based on AOMP, which is freely available at https://aomp.alphama.com.cn.

1. Introduction

Over 75% of the therapeutic agents currently on the market undergo phase 1 metabolism mediated by the cytochrome P450 (CYP450) enzyme[1]. Due to genetic polymorphism and susceptibility to induction and inhibition, P450 enzymes can cause individual medication differences and drug−drug interactions[2−4]. In contrast, drug interactions and individual medication differences caused by non-P450 oxidases are less frequently reported[5,6]. In recent years, more compounds that can potentially be metabolized by non-CYP450 enzymes have been designed and synthesized, and the role of the non-CYP450 metabolic enzymes in drug discovery has also become increasingly important[7,8]. Human aldehyde oxidase (hAOX, EC1.2.3.1) is an important non-CYP450 enzyme responsible for the biotransformation of numerous xenobiotics and therapeutic drugs. hAOX, which is mainly present in liver cytosol, uses molybdenum, flavin adenine dinucleotide, and Fe−S clusters for its catalytic function[9]. It has a wide range of substrate specificity and the capacity to catalyze multiple distinct metabolic reactions, including oxidations of aldehydes, oxidations of *N*-heterocycles, hydrolysis of amides, and various reductions[10]. Among these, the transformation of *N*-heterocycles to the corresponding oxo-*N*-heterocycles is the most concerning AOX-mediated metabolic reaction in drug discovery. It has contributed to the clinical failure of many novel agents, such as carbazeran, BIBX1382, FK3453, JNJ-38877605, and Lu AF09535[11−13]. These drugs are mainly kinase inhibitors, as their structures generally include nitrogen-containing heterocycles as important binding motifs, making them more likely to be liable to AOX-mediated metabolism[14−16]. Given the enormous losses caused by clinical development failures, it is essential to thoroughly evaluate AOX-mediated metabolism in the early drug discovery process[17]. However, *in vitro* and *in vivo* studies of AOX-mediated metabolism are costly and not applicable to compounds not yet synthesized. Therefore, *in silico* methods to predict AOX metabolism are urgently needed, allowing medicinal chemists to quickly assess the risk of compounds being metabolized by AOX in the early stage of drug discovery.

There are relatively few existing AOX metabolism prediction methods, and they have certain limitations[18]. In 2018, Gabriele et al. developed a computational method that predicts AOX metabolism based on molecular dynamics simulation, molecular docking, and quantum chemical calculation. This method was integrated into commercial software called MetaSite[19]. In 2020, we used deep neural networks to classify AOX substrates and non-substrates and decision tree models to predict site-of-metabolism (SOM). However, these machine learning (ML) models also relied on the molecular descriptors calculated by quantum chemistry[20]. The tedious and time-consuming molecular docking and quantum chemical calculation process greatly hinder the application of the above two methods in large-scale screening. In 2019, Marco et al. reported a method to determine the site-of-metabolism of AOX, where the aromatic carbon atom with the largest ^{13}C nuclear magnetic resonance (NMR) chemical shifts calculated by ChemDraw was predicted as the most likely metabolic site. This method can quickly determine the metabolic sites on a known AOX metabolic substrate, with an AUC of 0.90, but it cannot predict whether a compound is an AOX substrate. Therefore, there are still significant limitations in its application[20,21].

In this study, we proposed AOMP, a novel AOX metabolic prediction model based on graph neural networks (GNN)[22−24]. AOMP is designed to support high throughput screening and utilizes only 2D molecular topological graphs as input, without relying on computationally expensive descriptors. Unlike some previous work on drug metabolism prediction that regards substrate/non-substrate classification and SOM prediction as two independent tasks[20,25], AOMP unifies the two tasks into a single model, avoiding error accumulation and conflicting results. Specifically, AOMP first regards the prediction of SOMs as a graph node classification task. If at least one node on the molecular graph is predicted to be a SOM, the molecule is predicted to be a substrate of AOX oxidative metabolism. Otherwise, the molecule is predicted to be a non-substrate. The AOMP model is jointly trained on both molecular level task (substrate/non-substrate classification) and atomic level task (SOM prediction). Unifying these two tasks through this method enables more efficient utilization of information in the dataset, as atomic-level labels (SOM/non-SOM) are incorporated in the training of molecular-level (substrate/non-substrate) classifiers. Further test results confirm that this method leads to improved model performance.

Currently, the lack of training data is a significant obstacle to building an empirical model that can predict AOX metabolism. The publicly available AOX metabolism data comprises only a few hundred compounds. To overcome this difficulty, we adopted a transfer learning strategy based on previous research findings. These findings indicated that the ^{13}C-NMR chemical shift values of aromatic carbon atoms are related to their susceptibilities to AOX metabolism[11,21]. We pre-trained the AOMP model with chemical shift data and then fine-tuned it with AOX metabolism data (Fig. 1A). Our results demonstrated that this transfer learning strategy significantly improved the performance of the model. To our knowledge, this was the first instance of experimental NMR spectra data being used in the pre-training of molecular representations. Given the richness of NMR spectral data and its inherent correlation with the chemical environment of atoms, the pre-training strategy used in this study should have the potential to be extended to various molecular property prediction tasks.

To further demonstrate the performance of the proposed model and expand our knowledge of the chemical motif with high AOX susceptibility, we evaluated the AOX metabolism liability of common fragments in kinase inhibitors using AOMP. We also verified the calculation results by *in vitro* experiments. Ultimately,

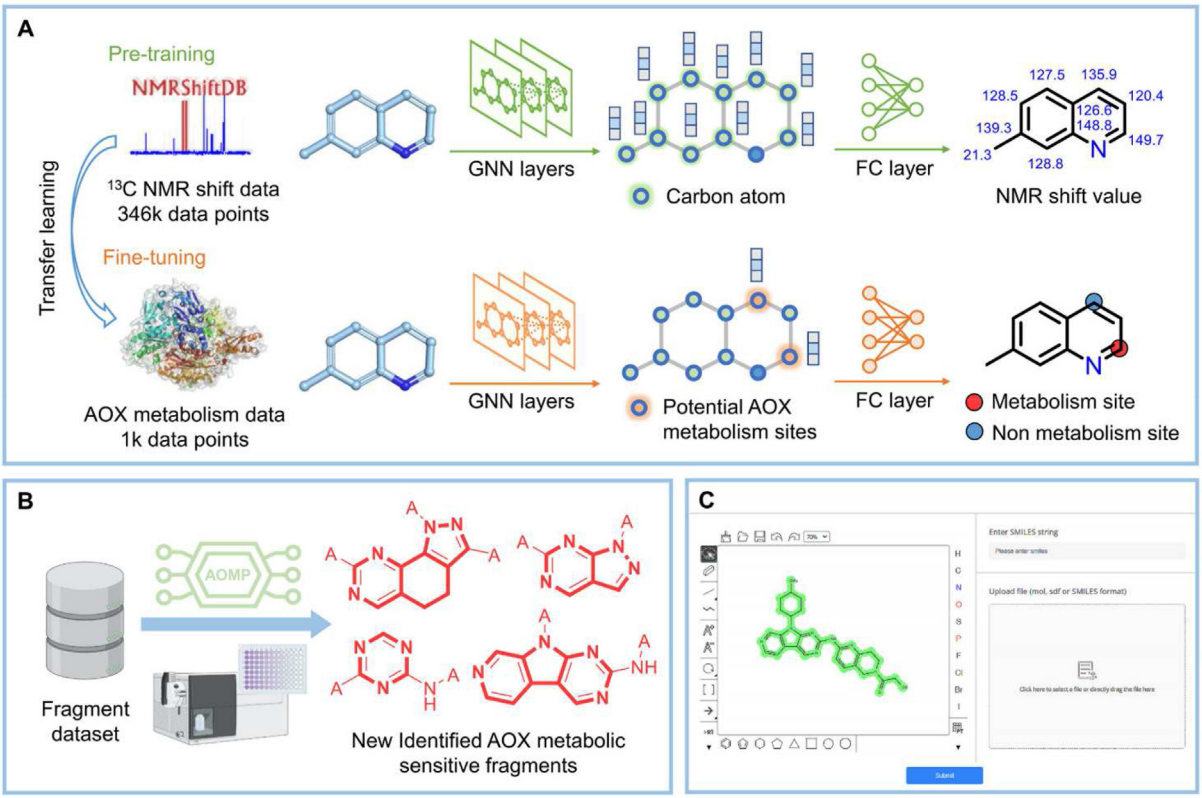

Figure 1 Overview of this work. (A) Schematic representation of the transfer learning pipeline. First, the large ^{13}C-NMR chemical shift dataset was used to train the graph neural network. This model was called the pre-trained model. Then, the AOX metabolic dataset was used to fine-tune the pre-trained model to establish the AOMP model. (B) Identification of novel AOX metabolic sensitive fragments through AOMP prediction and *in vitro* experiment verification. (C) Snapshot of the web-server interface of AOMP.

we revealed four novel *N*-heterocycles susceptible to AOX oxidative metabolism (Fig. 1B). These results suggest that special attention should be given to evaluating their susceptibility to AOX metabolism when designing kinase inhibitors containing such structures. Moreover, to enhance the accessibility of the AOMP model to the community, we have provided a web service for the AOMP model that is freely available at https://aomp.alphama.com.cn (Fig. 1C).

2. Results and discussion

2.1. *Overview of AOX metabolism data set*

Our training set consists of 203 substrates and 296 non-substrates of AOX oxidative metabolism, taken from the article of Gabriele et al.[19] The physical−chemical properties of molecules, such as Log*P* or Log*D*, are important determinants of their susceptibility to the CYP450 enzyme[26,27]. However, as shown in Fig. 2A and Supporting Information Fig. S1, there was no significant difference between the simple molecular properties of the substrate and non-substrate of AOX in the training set. This indicates that predicting AOX metabolism is a challenging task. The metabolic sites of all substrates in the training set are known, and there is a total of 324 SOMs. Based on the reaction mechanism and previous AOX oxidative metabolites[19,28], potential SOMs are defined as the para and ortho positions of the nitrogen atom in a six-membered aromatic heterocycle and the ortho position of the nitrogen atom in a five-membered aromatic heterocycle (Fig. 2B). Atoms within a molecule that belong to potential metabolic sites but are not SOMs are defined as non-SOMs, leading to a total of 755 non-SOMs in our training set. In addition to the training set, we compiled an external test set by combining data from 11 articles, which contain 47 substrates and 52 non-substrates of AOX oxidative metabolism. There are no identical molecules between the external test set and the training set. The maximum similarity of more than 70% of the molecules in the external test set to the training set molecules is less than 0.5 (Fig. 2C). Among the 47 substrates in the external test set, the metabolic sites of 27 substrates are known. There are a total of 30 SOMs and 187 non-SOMs in the external test set. Fig. 2D shows the potential SOMs of compounds in the training and external test set. The training and external test set data are available as Supporting Information.

2.2. *Overview of AOMP model*

The AOMP model was developed to unify the substrate/non-substrate classification and SOM prediction tasks. The architecture of the model is shown in Fig. 3. The model begins by describing each molecule as an undirected graph with atoms as nodes and bonds as edges. The representations of the graph are initialized with eight kinds of atom features and four kinds of bond features (Supporting Information Table S1). The initialized molecular graph is then input into the graph neural layers for message passing across atoms. AOMP includes two different

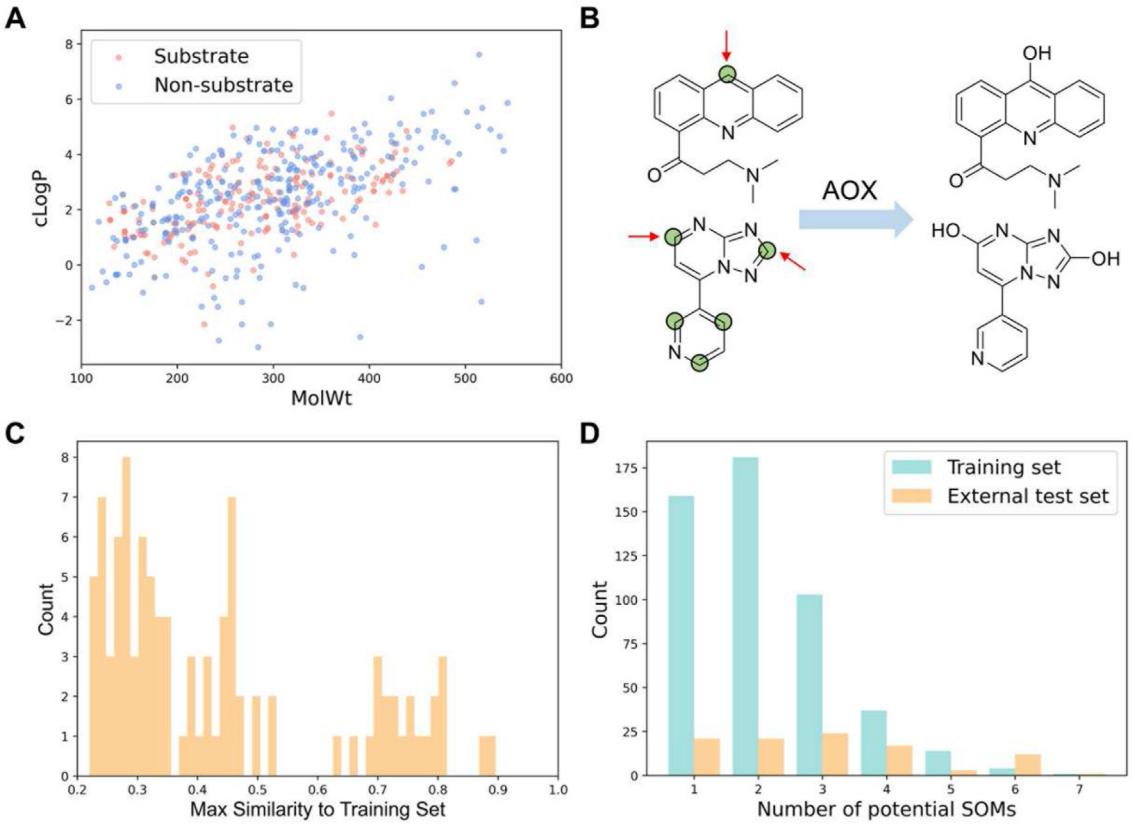

Figure 2 Overview of datasets. (A) The scatter plot of *c*Log*P versus* MolWt for the molecules in the training set. (B) Examples of oxidative metabolic substrates and metabolites of AOX are shown, with potential metabolic sites defined by empirical rules (marked by green circles). Only some of these sites are actually observed to be oxidized (marked by arrow). (C) The distribution of the maximum similarity of molecules in the external test set to molecules in the training set. (D) The distribution of the number of potential metabolic sites of molecules in the training and external test set.

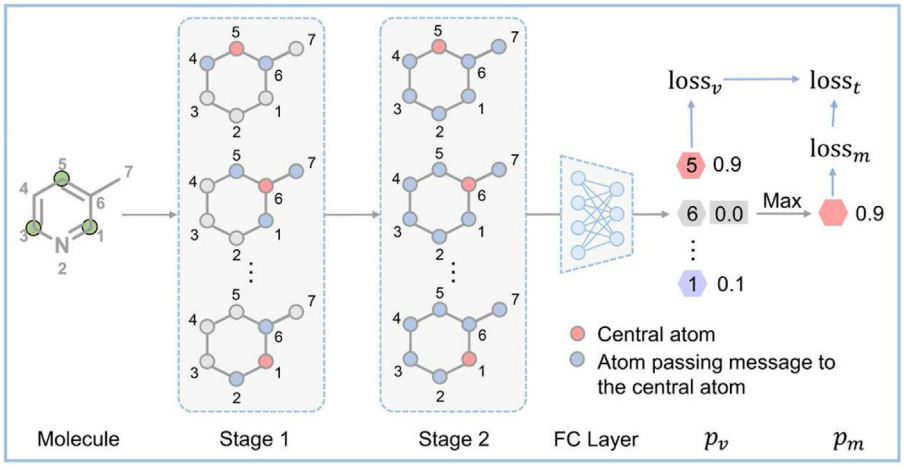

Figure 3 The architecture diagram for AOMP model.

message passing stages. The first stage is the message passing between neighbor atoms, which is designed to learn the local information of atoms. The second stage is the message passing between all atoms in the molecule, which is designed to capture the interaction between two atoms that are relatively distant on the graph. After the message passing stage, the feature vectors of all atoms are fed into a fully connected (FC) layer to predict their probabilities of being metabolized. The maximum probability of atoms in a molecule being SOMs is taken as the probability of this molecule being a metabolic substrate. Based on this framework, AOMP can simultaneously perform substrate/non-substrate classification task and SOM prediction task. To train the proposed model, we formulate a mixed loss ($loss_t$). It consists of two parts ($loss_v$ and $loss_m$): one for SOM/no-SOM classification and the other for substrate/no-substrate classification tasks, respectively. To further enhance the model, the transfer learning strategy was

adopted. The AOMP model was first pre-trained with the ^{13}C-NMR chemical shift data of 25,000 molecules obtained from nmrshiftdb2 and then fine-tuned on the AOX metabolism data (for more details about the model architecture and transfer learning strategy, see Experimental Section).

2.3. *Performances of AOMP on cross-validation*

To evaluate the performance of AOMP, four conventional ML models and a GNN model (Attentive FP) were implemented as baseline methods[29]. The performance of AOMP and other models was first evaluated on the training set using 5 times 5-fold cross-validation. As shown in Table 1, AOMP outperformed all other baseline models in terms of AUC, accuracy, and sensitivity on the task of substrate/non-substrate classification. Although the precision of the RF model is slightly higher than that of AOMP, its sensitivity is significantly lower than AOMP. In addition to classifying substrates and non-substrates, AOMP can accurately distinguish metabolic sites from non-metabolic sites. This not only provides an explanation for the results of substrate/non-substrate classification, but also offers useful guidance for medicinal chemists to manipulate AOX-mediated metabolism liability for structure optimization or prodrug design. To better comprehend the exceptional performance of AOMP, ablation experiments were performed to evaluate the performances of the AOMP model without chemical shift data pre-training (AOMP_noPretrain) and the AOMP model trained without information on metabolic sites (AOMP_noAtomLabel). The results revealed that the pre-training with chemical shift data considerably improved the performance of the model. Additionally, training with atomic level labels during model fine-tuning was not only beneficial to the performance of the model on SOMs prediction, but also to the substrate/non-substrate classification. This indicates that the information of metabolic sites is crucial and helpful for substrate/non-substrate classification. However, this information was typically overlooked in previous studies on the substrate/non-substrate classification of various metabolic enzymes[20,25,30].

2.4. *Performances of AOMP on external test*

To verify the generalizability of AOMP, we further test it on the external test set. As shown in Table 2, AOMP outperformed other baseline models and ablation models in all evaluation indicators and tasks. We further conducted a grouped analysis of the external test set. We divided the external test set into three subsets based on their maximum similarity to the molecules in the training set. As shown in the Supporting Information Fig. S2. AOMP model performed well in different similarity subsets, indicating its good generalizability and robustness. Since the ^{13}C-NMR chemical shift calculated by ChemDraw was regarded as a useful indicator to distinguish SOMs from non-SOMs of AOX, we also evaluated it on the external test set. According to Youden's index[31], the threshold of the chemical shift to classify an atom as either SOM or non-SOM was determined to be 145.9 ppm. In addition, we also tried to distinguish the substrate from the non-substrate by using the maximum chemical shift of potential metabolic sites on molecules. The results showed that the chemical shift calculated by ChemDraw achieved an AUC of 0.790 in distinguishing metabolic sites from non-metabolic sites, but performed poorly in determining the propensity of the compound to be an AOX substrate, which is consistent with our previous reports[20]. Moreover, we evaluated the performance of the chemical shift calculated by our pre-trained model, which was only trained with the chemical shift dataset and not fine-tuned with the AOX dataset. In the SOM/non-SOM classification task, the chemical shift predicted by our pre-trained model performed comparably with that by ChemDraw, and in the substrate/non-substrate classification task, the chemical shift predicted by our pre-trained model was slightly better than that by ChemDraw.

In addition, we compared AOMP to our previously reported model on the external test set consisting of 27 molecules[20]. As shown in Supporting Information Table S2, AOMP and our previous model exhibited comparable performance, correctly predicting the AOX metabolism liability for 25 and 24 molecules, respectively. Upon examination of the quantitative metabolic data of these molecules, we found that the three molecules incorrectly predicted by AOMP all exhibited very weak metabolic activity (Fig. 4). This suggests that the identification of these molecules as either substrates or non-substrates may be ambiguous depending on the detection method used and the selected threshold. Hence, the misclassification of those molecules by the computational model should be acceptable. However, this also indicates the limitation of the binary classification model in predicting borderline molecules between metabolic classification groups. Developing quantitative metabolic prediction models is thus an important research direction for the future.

2.5. *Influences of pre-training and fine-tuning*

To better understand the influence of pre-training and fine-tuning on our model, we compared the predicted metabolic probability with AOMP and the calculated ^{13}C-NMR shift with our pre-trained model for all potential metabolic sites in the external

Table 1 Performances of AOMP and other models on the five-fold cross-validation (bold represents the best result).

Task	Method	AUC	Accuracy	Sensitivity	Precision
Substrate/non-substrate classification	KNN	0.749	0.740	0.596	0.725
	SVM	0.852	0.804	0.757	0.766
	RF	0.866	0.795	0.660	**0.804**
	ANN	0.835	0.776	0.700	0.740
	Attentive FP	0.830	0.760	0.763	0.689
	AOMP	**0.909**	**0.847**	**0.858**	0.790
	AOMP_noPretrain	0.862	0.803	0.805	0.745
	AOMP_noAtomLabel	0.890	0.823	0.819	0.768
SOM/non-SOM classification	AOMP	**0.918**	**0.877**	**0.814**	**0.784**
	AOMP_noPretrain	0.866	0.825	0.674	0.728
	AOMP_noAtomLabel	0.846	0.787	0.758	0.617

Table 2 Performances of AOMP and other models on the external test set (bold represents the best result).

Task	Method	AUC	Accuracy	Sensitivity	Precision
Substrate/non-substrate classification	KNN	0.635	0.616	0.553	0.604
	SVM	0.810	0.727	0.723	0.708
	RF	0.831	0.721	0.613	0.754
	ANN	0.739	0.689	0.570	0.717
	Attentive FP	0.817	0.756	0.736	0.744
	AOMP	**0.881**	**0.816**	0.774	**0.827**
	AOMP_noPretrain	0.854	0.786	0.736	0.798
	AOMP_noAtomLabel	0.849	0.766	0.702	0.782
	NMR shift (ChemDraw)	0.648	0.636	**0.830**	0.582
	NMR shift (Ours)	0.682	0.646	**0.830**	0.591
SOM/non-SOM classification	AOMP	**0.892**	**0.882**	**0.907**	**0.544**
	AOMP_noPretrain	0.789	0.849	0.707	0.470
	AOMP_noAtomLabel	0.815	0.835	0.787	0.450
	NMR shift (ChemDraw)	0.790	0.714	0.767	0.295
	NMR shift (Ours)	0.780	0.691	0.733	0.272

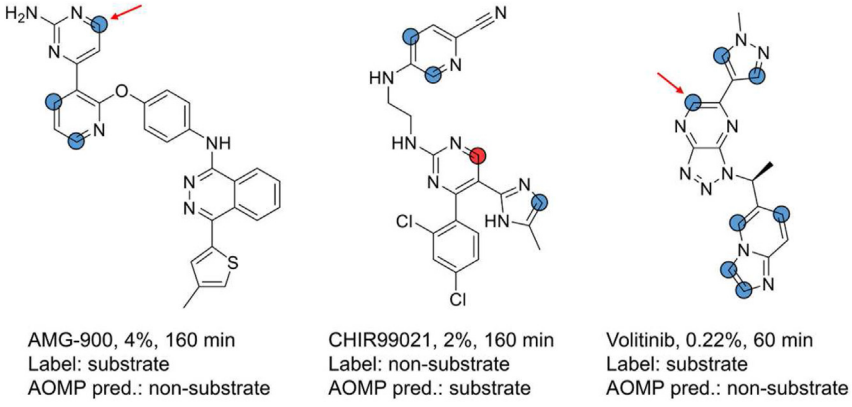

Figure 4 Three molecules incorrectly predicted by AOMP. The percentages refer to the ratio of metabolites measured by *in vitro* experiments, and the time refers to the incubation time of metabolic measurements[16,32]. The red arrows denote the SOMs determined by *in vitro* experiment, and the red and blue circles denote the SOMs and non-SOMs predicted by AOMP.

test set (Fig. 5A). It can be noted that the potential sites whose calculated chemical shifts are less than 135 ppm are hard to metabolize. This is because the AOX-mediated oxidative metabolism relies on the electrophilicity of the carbon at the site of reaction, while the ^{13}C-NMR chemical shift values can well reflect the electrophilicity of carbons[33,34]. The embeddings in the last hidden layer of the pre-trained model were extracted and submitted to principal component analysis (PCA). As shown in Fig. 5D, the embeddings of the SOMs are more distributed on the lower left of the figure compared with the embeddings of the non-SOMs. In contrast, in the randomly initialized model, the distributions of SOMs and non-SOMs are highly consistent (Fig. 5C). The above finding explains why the chemical shift can be used as an indicator to evaluate the susceptibility of the potential SOMs to AOX and why the pre-training with the NMR shift data is beneficial to our AOMP model. However, for a carbon atom to be a SOM, it is not enough to only possess large electrophilicity (chemical shift). The atom should also satisfy many other conditions such as being accessible to the molybdenum catalytic center of AOX. Therefore, although the calculated NMR shift of some atoms is very high, they are still non-SOMs. We believe that the AOMP model can learn other factors affecting the metabolism liability of atoms in the fine-tuning stage to make more accurate predictions than the pre-trained model. Some specific examples are shown in Fig. 5B. Although the pre-trained model predicted high NMR shift values for these sites, the AOMP model after the fine-tuning still correctly predicted them as non-SOMs. Fig. 5E also showed that after fine-tuning, the embeddings of SOMs and non-SOMs were more significantly separated.

2.6. *Assessing AOX metabolism liability of common fragments in kinase inhibitors*

Kinase inhibitors are a crucial class of therapeutics, accounting for a quarter of all current drug discovery research and development pipelines[35–37]. Most kinase inhibitors possess nitrogen heterocyclic structures, which bind with the hinge region of the kinase, making them vulnerable to AOX metabolism. To evaluate the AOX metabolism risk of kinase inhibitors and provide guidance for drug design and development, we used AOMP to systematically analyze the common hinge region-binding fragments of existing kinase inhibitors.

The kinase hinge-binding fragments set used in this study was summarized by Zhang et al., and it contained a total of 767 fragments[38]. Fragments that contained multiple ring systems were removed, leaving 670 fragments, of which 409 had potential AOX oxidative metabolic sites. Since many fragments are highly similar

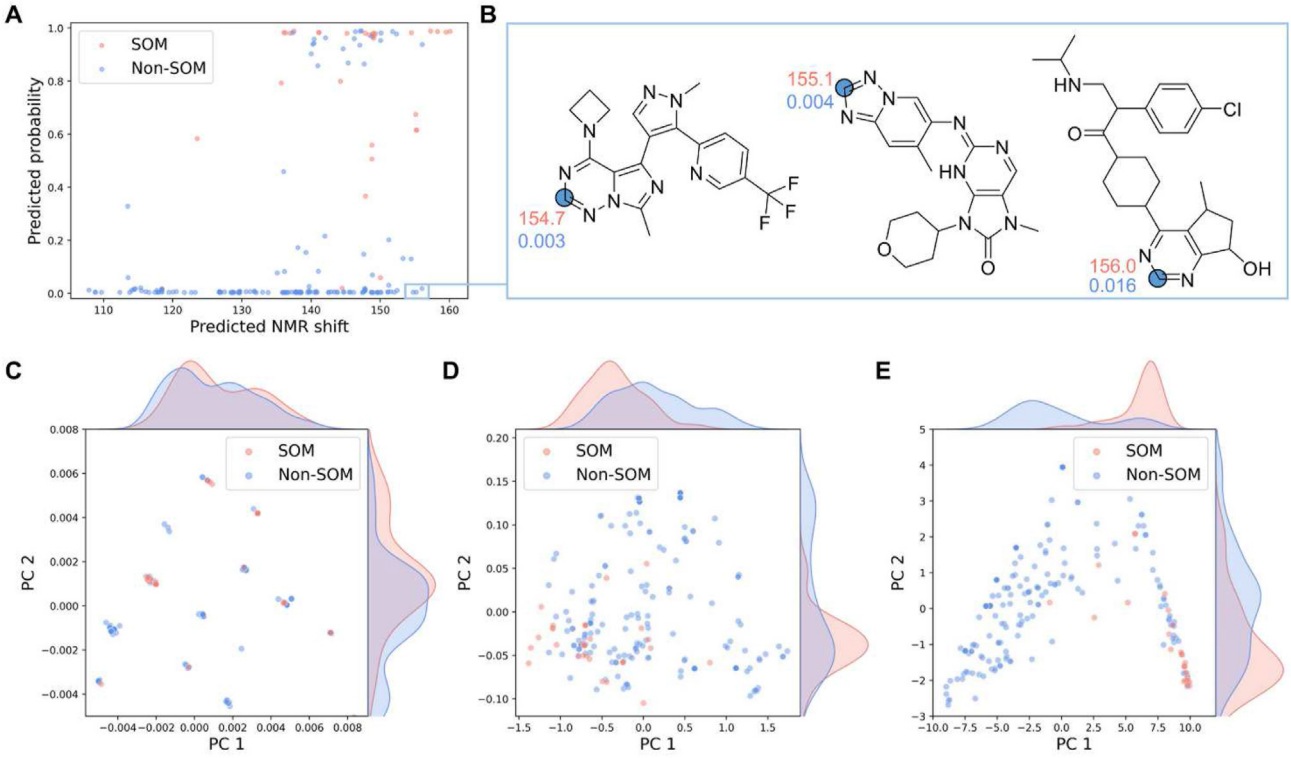

Figure 5 Analysis of the role of pre-training and fine-tuning. (A) A scatter plot that shows the predicted NMR shift *vs*. predicted probability for the external test set. (B) Examples of molecules in the external test set, along with the prediction results of the pre-trained model and AOMP. The red numbers represent the predicted chemical shift, and the blue numbers represent the predicted probability of being SOMs. (C−E) A visualization of the atomic embeddings of the randomly initialized (C), pre-trained (D), and fine-tuned model (E) with principal component analysis.

and share the same heterocyclic cores, we only retained 156 unique heterocyclic cores with potential SOMs. Of these, 24 heterocyclic cores (about 15%) were reported to be liable to AOX metabolism.

Using AOMP, we evaluated the AOX metabolism liability of the remaining 132 heterocyclic cores that had not been reported to be metabolized by aldehyde oxidase, corresponding to a total of 248 fragments. Since AOMP could not directly predict the metabolism liability of fragments, we first matched these fragments with the existing kinase inhibitors in BindingDB[39], and then predicted whether these kinase inhibitors would be metabolized by AOX at the matched fragments. The prediction results were presented in Supplementary Information. A fragment was considered to have a high metabolic risk when more than 30% of kinase inhibitors containing the fragment were predicted to be metabolic substrates. A fragment was disregarded if it appeared less than 20 times in the kinase inhibitors. Finally, we discovered 23 high-risk fragments containing 15 unique heterocyclic cores. These fragments could serve as structural alerts, providing guidance for drug screening and design. Based on the accessibility of compounds, we selected seven fragments for experimental verification and identified four new AOX metabolic-sensitive fragments that didn't exist in any known aldehyde oxidase substrate (Fig. 6A).

Fig. 6B shows the structures of the seven fragments, along with the proportion that kinase inhibitors containing these fragments are predicted as AOX substrates. The four newly identified AOX metabolic-sensitive fragments are highlighted in red. It is worth noting that these four fragments also have the highest predicted metabolic probability among the seven. We selected four representative molecules for *in vitro* experiment for the three fragments with lower predicted metabolic probability, but their metabolites were not detected. This result demonstrates the good ranking and uncertainty evaluation abilities of AOMP, as the confidence in the prediction decreases with a less reliable prediction result. However, this result does not exclude the possibility of AOX metabolism in these three fragments due to the small sample size for experimental evaluation.

Fig. 6C shows the 14 representative molecules that were selected for *in vitro* metabolism experiments. The susceptibility of these compounds to AOX was determined using a human liver cytosol assay. All compounds were incubated in an environment containing AOX (liver cytosol) and monitored for substrate loss and the formation of oxidative metabolites. As shown in Table 3 and Supporting Information Figs. S3−S13, ten molecules (A-1−3, B-1−5, C-1, and D-1) demonstrated both parent loss and oxidative metabolite formation, suggesting that they might be AOX substrates. To eliminate interference from xanthine oxidase (XO), another enzyme presented in the liver cytosol, specific enzyme inhibitors were added to the incubation system. The AOX inhibitors, raloxifene and hydralazine, inhibited over 71.5% of oxidative metabolites formation of the above potential substrate molecules, while the XO inhibitor, allopurinol, displayed limited inhibition (less than 23.9%). Therefore, A-1−3, B-1−5, C-1, and D-1 were confirmed to be AOX substrates.

2.7. *AOMP web service*

For the convenience of no-code users, we have developed a web server that wraps the AOMP model at https://aomp.alphama.com.cn. This web server accepts various types of inputs, including

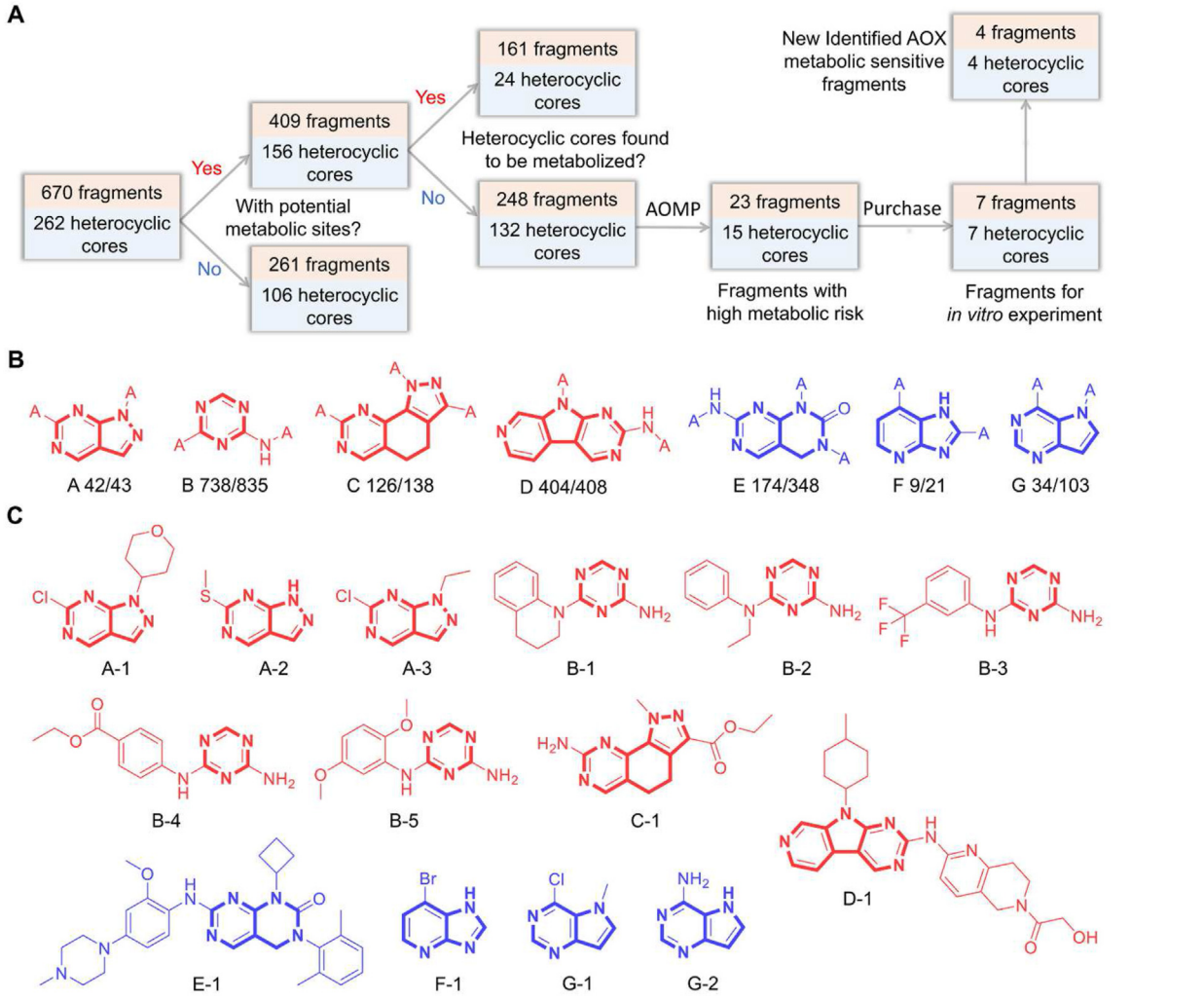

Figure 6 Assessing AOX metabolism liability of common fragments in kinase inhibitors by AOMP. (A) The overall workflow of discovering new metabolic-sensitive fragments for AOX. (B) Seven fragments were selected, metabolic and non-metabolic fragments are colored red and blue, respectively. The fractions refer to the proportion that kinase inhibitors containing these fragments are predicted as AOX substrates. (C) Representative compounds containing the selected fragments, where the substrates are shown in red and non-substrates in blue.

drawing a molecule from the embedded molecular editor, pasting SMILES, or uploading a molecule structure file with txt/mol/sdf formats. The AOMP web service provides batch calculation functionality, with a maximum of 5000 molecules that can be submitted at one time. On our web server, the prediction of 5000 molecules can be completed within 20 min. The calculation results from the AOMP website can be displayed online and downloaded. These results include a molecule image labeled with atom indexes and a table recording the predicted metabolic probabilities and ^{13}C-NMR shift values. Up to 30 molecules can be displayed online simultaneously. With its high accuracy, rapid processing, and user-friendly interface, AOMP can serve as a convenient and practical tool to assist in drug screening and design work.

The AOMP web's implementation is based on the standard B/S architecture, which separates the front and back ends. For the back end, MySQL is used for persistent data storage, Redis acts as an in-memory data store, RabbitMQ is deployed as the message broker, and a Spring Boot platform is created for all modules to interact. As for the front end, apart from the Vue. js module, we also use the Element UI toolkit for building the web components.

The AOMP web service is freely accessible to all users without any login privileges required. To ensure the security and privacy of users' data, the AOMP web server does not retain any data from users and provides only the AOMP computing service.

3. Conclusions

In this study, we introduced AOMP, a novel graph neural network model for predicting AOX-mediated metabolism. AOMP not only classifies metabolic substrates and non-substrates but also predicts metabolic sites. Unlike previous methods that relied on time-consuming molecular docking or quantum chemical calculations, AOMP only requires molecular graphs as input, allowing for large-scale screening and molecular design. The AOMP model has three main innovative features. First, it represents a new learning paradigm that unifies atomic-level classification tasks with related molecular-level classifications, and can serve as a universal framework for predicting various enzyme metabolisms. Secondly, it has demonstrated the potential of NMR shift data in enhancing neural networks' understanding of molecular properties, thereby pointing out a promising new direction for the development of

Table 3 Identification of hAOX substrates using a liver cytosol assay (oxidative transformation).

Compd.	$t_{1/2}$ (h)	Presence of [O]-metabolite	Raloxifene inhibition ratio (%)	Hydralazine inhibition ratio (%)	Allopurinol inhibition ratio (%)
A-1	0.102	Y	94.2	77.8	7.15
A-2	0.263	Y	98.4	92.5	2.74
A-3	0.347	Y	96.5	95.8	1.90
B-1	4.69	Y	98.7	97.3	4.84
B-2	9.11	Y	99.3	98.9	23.9
B-3	0.824	Y	76.8	76.7	14.0
B-4	0.343	Y	71.5	85.7	21.9
B-5	0.758	Y	99.4	96.4	1.27
C-1	0.129	Y	99.6	99.5	2.04
D-1	6.01	Y	99.3	99.0	22.1
E-1	13.4	N	–	–	–
F-1	8.46	N	–	–	–
G-1	26.5	N	–	–	–
G-2	15.7	N	–	–	–
*O*6-Benzylguanine (positive control)	1.44	Y	99.4	98.8	21.1

molecular representation learning and small molecule pre-training models. Finally, the AOMP model can be accessed through a web server (https://aomp.alphama.com.cn), serving the community for accurate, fast, and convenient prediction of AOX metabolism. We evaluated the AOX metabolism liability of prevalent fragments in kinase inhibitors with AOMP model. The results were validated through *in vitro* experiments, leading to the discovery of four novel *N*-heterocycles prone to AOX metabolism. This discovery expands our understanding of chemical motifs with high AOX susceptibility and can provide guidance for the design and modification of kinase inhibitors.

4. Experimental

4.1. Model architecture

AOMP is a variant of Attentive FP that we previously developed[29]. It has seven GNN layers, with the first six layers are used for the message passing in Stage 1 and the last layer is used for the message passing in Stage 2 (Fig. 3). They can be written as Eqs. (1) and (2):

Stage 1:

$$h_v^k = \mathrm{GRU}^{k-1}\left(\sum_{u\in N(v)} M^{k-1}\left(h_u^{k-1}, h_v^{k-1}\right), h_v^{k-1}\right) \tag{1}$$

Stage 2:

$$h_v^{k+1} = \mathrm{GRU}^{k}\left(\sum_{u\in E(v)} M^{k}\left(h_u^{k}, h_v^{k}\right), h_v^{k}\right) \tag{2}$$

where h_v^i is the feature vector of target atom v after k iterations, $N(v)$ represents all neighbor atoms of atom v, and $E(v)$ represents all atoms in the molecule except atom v. M^{k-1} is the message function at iteration $k-1$, which is the same as the message function in Attentive FP. GRU^{k-1} is a gated recurrent unit used as the update function at iteration $k-1$.

Following the GNN layers, a FC layer is implemented to predict the metabolic probabilities of atoms, which is activated by a sigmoid function. The metabolic probabilities of non-potential metabolic sites are then masked with zero. Next, the maximum of the metabolic probabilities of all atoms is calculated, and taken as the probability of this molecule being a metabolic substrate. For an atom v with features h_v^K and in molecule G, the above process can be written as Eqs. (3)–(5):

$$p_v = \mathrm{Sigmoid}\left(\mathrm{FC}\left(h_v^K\right)\right) \tag{3}$$

$$p_v = \begin{cases} p_v,\ p_v \in Q \\ 0,\ p_v \notin Q \end{cases} \tag{4}$$

$$p_m = \max\left(\{p_v | v \in G\}\right) \tag{5}$$

where FC is referred to a fully connected neural network layer, Q is the potential metabolic sites, p_v is the probability of atom v being a SOM, and p_m is the probability of molecule G being an AOX substrate.

Both the SOM/no-SOM classification task and the substrate/no-substrate classification task in the AOMP model use binary cross-entropy as the loss function (loss_v and loss_m). To optimize the model, the mean of the two binary cross-entropy losses is used as the total loss (loss_t). For the ablation model AOMP_noAtomLabel, the loss only consists of loss_m and can be regarded as a multi-instance learning model that learns the labels of atoms through training against the labels of molecules[40–42]. The computational methods of loss_v, loss_m, and loss_t are shown as Eqs. (6)–(8):

$$\mathrm{loss}_v = -\frac{1}{N}\sum_{i=1}^{N} y_i \cdot \log(p_v) + (1-y_i)\cdot\log(1-p_v) \tag{6}$$

$$\mathrm{loss}_m = -\frac{1}{M}\sum_{j=1}^{M} y_j \cdot \log(p_m) + \left(1-y_j\right)\cdot\log(1-p_m) \tag{7}$$

$$\mathrm{loss}_t = \frac{\mathrm{loss}_v + \mathrm{loss}_m}{2} \tag{8}$$

where N and M refer to the number of potential metabolic sites and molecules in training samples, respectively, while y_i and y_j refer to the corresponding labels.

4.2. Transfer learning strategy

The ^{13}C-NMR chemical shift data used for pre-training was obtained from nmrshiftdb2 (https://nmrshiftdb.nmr.uni-koeln.de/). After pretreatment, there were 32,470 molecules and 345,836 ^{13}C-NMR shift values. Of these, 25,000 molecules were randomly split into the training set and the remaining 7470 molecules were kept as the validation set. Since the chemical shifts of atoms mainly depend on the local environment around them, only message passing between neighbor atoms (Stage 1) was carried out to extract atomic features during the pre-training. The learned atom features were then fed into a fully connected layer to predict their chemical shift values. The mean absolute error of our pre-training model on the validation set is 0.139 (Supporting Information Fig. S14), which is equivalent to the performance of the previously reported model for ^{13}C-NMR shift prediction[43]. During fine-tuning, the weights of the AOMP model in the first message passing stage (Stage 1) and readout stage were initialized with the weight of the pre-trained model, while the weights in the second message passing stage (Stage 2) were randomly initialized. The AOX metabolic data set was used to train our model and generate the final prediction model.

4.3. Model implementation and evaluation

The AOMP and Attentive FP model were implemented with PyTorch framework and DGL package. The DGL-LifeSci package[44] was used to calculate the initial features of molecular graphs. Four machine learning models, including support vector machine (SVM), random forest (RF), artificial neural network (ANN) and K-nearest neighbor (KNN) were implemented using the Scikit-learn package. The input of machine learning model was the 2048-bit Morgan2 fingerprints calculated using the RDKit package. To find their optimal parameter settings and assess their internal validity, the AOMP model and other baseline models were first trained by performing five times five-fold cross-validation in the training set. Then, all models were retrained with the whole training set under optimal hyperparameters determined in five-fold cross-validation and evaluated on the external dataset through five independent runs. The performance metrics for evaluating the model are AUC (area under the ROC curve), Accuracy, Sensitivity, and Precision. AUC is the area under the receiver operating characteristic curve, where the true positive rate against the false positive rate is plotted. The other three metrics are calculated with Eqs. (9)−(11):

$$\text{Accuracy} = \frac{\text{TN} + \text{TP}}{\text{TN} + \text{TP} + \text{FP} + \text{FN}} \tag{9}$$

$$\text{Sensitive} = \frac{\text{TP}}{\text{TP} + \text{FN}} \tag{10}$$

$$\text{Precision} = \frac{\text{TP}}{\text{TP} + \text{FP}} \tag{11}$$

where TN, TP, FN, and FP are the numbers of true negatives, true positives, false negatives, and false positives, respectively.

4.4. Data collection and preparation

Our training data was extracted from the dataset of Gabriele et al.[29], which contained 513 molecules with AOX oxidative metabolism data. We removed 15 of these molecules due to inconsistent experimental results with other reports or a lack of potential metabolic sites. The external test set was manually collected from 11 articles, and only experimental data from human hepatocytes was adopted. For molecules that were not explicitly marked as substrate or non-substrate in the original literature, we divided them into substrate and non-substrate using a half-life of 500 min as a threshold. For some substrate molecules, certain atoms were topologically equivalent. In such cases, if one atom underwent oxidative metabolism, all atoms were labeled as metabolic sites (Supporting Information Fig. S15). To obtain kinase inhibitors, we downloaded the BindingDB database and used a list of UniProt IDs of kinase proteins to retrieve kinase inhibitors from it. We found a total of 187,371 kinase inhibitors (Supporting Information). The structures of all molecules were standardized by removing salts, neutralizing charge, and normalizing tautomer.

4.5. Metabolic stability study

We used parent compound depletion in human liver cytosolic incubation to measure metabolic stability. The tested compounds were purchased from TopScience (Shanghai, China) and Bidepharm (Shanghai, China) without further purification. The human liver cytosol (mixed sex; a pool of 50 donors; catalog no. H0610.C, lot no. 1610027; 30 males and 20 females) was purchased from Sekisui XenoTech. The incubation mixture had a total volume of 200 μL and consisted of human liver cytosol (2 mg/mL final protein concentration), 2 mmol/L $MgCl_2$, 1 μmol/L test compound, and 100 mmol/L potassium phosphate buffer, pH 7.4. The final DMSO concentration used in the assay was less than 0.1% (*v*/*v*). We pre-warmed the mixture at 37 °C for 5 min in a low-speed shaking thermomixer before adding the test compound. After incubation, we removed a 30 μL sample aliquot at 0, 0.25, 0.5, 1, 2, and 3 h, and quenched it with 300 μL acetonitrile. We immediately mixed each sample and then centrifuged it at 13,000 rpm for 10 min at room temperature. We diluted the supernatant with acetonitrile/water (1/1, *v*/*v*) and transferred it into a 96-well plate for analysis by LC−MS/MS. The control samples were prepared with no test compound or with inactivated enzymes. The LC−MS/MS analysis method is described in Supporting Information.

4.6. Molybdenum hydroxylase inhibition study

In this study, aldehyde oxidase selective inhibitors raloxifene and hydralazine, and xanthine oxidase selective inhibitor allopurinol were used to investigate the involvement of human aldehyde oxidase in the oxidative metabolism of the test compounds. The incubation system was similar to the one used in the metabolic stability study described above. Specifically, it contained human liver cytosol (2 mg/mL final protein concentration), 2 mmol/L $MgCl_2$, 1 μmol/L test compound, 100 μmol/L inhibitor, and 100 mmol/L potassium phosphate buffer, pH 7.4. The test compounds and inhibitors were dissolved in DMSO, respectively, and the final concentration of DMSO in each incubation (100 μL total volume) was less than 1.1% (*v*/*v*). The mixtures were preincubated for 5 min at 37 °C, and each reaction was initiated by adding a test compound. After incubating for 3 h at 37 °C, the reactions were terminated by adding 1000 μL of acetonitrile. The mixtures were centrifuged and the supernatants were diluted with a certain proportion of acetonitrile/water (1/1, *v*/*v*) and transferred into a 96-well plate for analysis by LC−MS/MS. Controls without

inhibitors were also prepared. The inhibition ratio of formation of oxidative metabolite was calculated using Eq. (12):

$$\text{Inhibition ratio} = 1 - \frac{A_W}{A_O} \quad (12)$$

where A_W and A_O refer to the peak area of oxidative metabolite in human liver cytosol with inhibitor and without inhibitor, respectively.

Acknowledgments

This work was supported by the National Natural Science Foundation of China (T2225002, 82273855 to Mingyue Zheng), Lingang Laboratory (LG202102-01-02 to Mingyue Zheng), the National Key Research and Development Program of China (2022YFC3400504 to Mingyue Zheng), the open fund of state key laboratory of Pharmaceutical Biotechnology, Nanjing University, China (KF-202301 to Mingyue Zheng).

Author contributions

Jiacheng Xiong designed the algorithm, conducted computational experiments, and drafted the manuscript. Rongrong Cui conducted *in vitro* experiments. Zhaojun Li built the web service. Wei Zhang and Zunyun Fun helped prepare the datasets. Runze Zhang, Xiaohong Liu, and Zhenghao Li helped check and improve and manuscript. Mingyue Zheng and Kaixian Chen led the project. All authors read and approved the final manuscript.

Conflicts of interest

The authors declare that they have no competing interests.

Appendix A. Supporting information

Supporting data to this article can be found online at https://doi.org/10.1016/j.apsb.2023.10.008.

References

1. Zanger UM, Schwab M. Cytochrome P450 enzymes in drug metabolism: regulation of gene expression, enzyme activities, and impact of genetic variation. *Pharmacol Ther* 2013;**138**:103–41.
2. Tanaka E. Clinically important pharmacokinetic drug–drug interactions: role of cytochrome P450 enzymes. *J Clin Pharm Therapeut* 1998;**23**:403–16.
3. Tang C, Lin JH, Lu AY. Metabolism-based drug–drug interactions: what determines individual variability in cytochrome P450 induction? *Drug Metab Dispos* 2005;**33**:603–13.
4. Manikandan P, Nagini S. Cytochrome P450 structure, function and clinical significance: a review. *Curr Drug Targets* 2018;**19**:38–54.
5. Zhou ZW, Chen XW, Sneed KB, Yang YX, Zhang X, He ZX, et al. Clinical association between pharmacogenomics and adverse drug reactions. *Drugs* 2015;**75**:589–631.
6. Pang X, Tang C, Guo R, Chen X. Non-cytochrome P450 enzymes involved in the oxidative metabolism of xenobiotics: focus on the regulation of gene expression and enzyme activity. *Pharmacol Ther* 2022;**233**:108020.
7. Hutzler JM, Obach RS, Dalvie D, Zientek MA. Strategies for a comprehensive understanding of metabolism by aldehyde oxidase. *Expert Opin Drug Met* 2013;**9**:153–68.
8. Lepri S, Ceccarelli M, Milani N, Tortorella S, Cucco A, Valeri A, et al. Structure–metabolism relationships in human-AOX: chemical insights from a large database of aza-aromatic and amide compounds. *Proc Natl Acad Sci U S A* 2017;**114**:E3178–87.
9. Coelho C, Foti A, Hartmann T, Santos-Silva T, Leimkühler S, Romão MJ. Structural insights into xenobiotic and inhibitor binding to human aldehyde oxidase. *Nat Chem Biol* 2015;**11**:779–83.
10. Coelho C, Garattini E, Leimkuehler S, Mota C, Romao MJ, Santos-Silva T, et al. Critical overview on the structure and metabolism of human aldehyde oxidase and its role in pharmacokinetics. *Coord Chem Rev* 2018;**368**:35–59.
11. Manevski N, King L, Pitt WR, Lecomte F, Toselli F. Metabolism by aldehyde oxidase: drug design and complementary approaches to challenges in drug discovery. *J Med Chem* 2019;**62**:10955–94.
12. Rashidi M-R, Soltani S. An overview of aldehyde oxidase: an enzyme of emerging importance in novel drug discovery. *Expet Opin Drug Discov* 2017;**12**:305–16.
13. Gajula SNR, Nathani TN, Patil RM, Talari S, Sonti R. Aldehyde oxidase mediated drug metabolism: an underpredicted obstacle in drug discovery and development. *Drug Metab Rev* 2022;**54**:427–48.
14. Wellaway CR, Baldwin IR, Bamborough P, Barker D, Bartholomew MA, Chung C, et al. Investigation of Janus kinase (JAK) inhibitors for lung delivery and the importance of aldehyde oxidase metabolism. *J Med Chem* 2021;**65**:633–64.
15. Zhang JW, Xiao W, Gao ZT, Yu ZT, Zhang JY. Metabolism of c-Met kinase inhibitors containing quinoline by aldehyde oxidase, electron donating, and steric hindrance effect. *Drug Metab Dispos* 2018;**46**:1847–55.
16. Dick RA. Refinement of *in vitro* methods for identification of aldehyde oxidase substrates reveals metabolites of kinase inhibitors. *Drug Metab Dispos* 2018;**46**:846–59.
17. Lai Y, Chu X, Di L, Gao W, Guo Y, Liu X, et al. Recent advances in the translation of drug metabolism and pharmacokinetics science for drug discovery and development. *Acta Pharm Sin B* 2022;**12**:2751–77.
18. Soltani S, Hallaj-Nezhadi S, Rashidi MR. A comprehensive review of in silico approaches for the prediction and modulation of aldehyde oxidase-mediated drug metabolism: the current features, challenges and future perspectives. *Eur J Med Chem* 2021;**222**:113559.
19. Cruciani G, Milani N, Benedetti P, Lepri S, Cesarini L, Baroni M, et al. From experiments to a fast easy-to-use computational methodology to predict human aldehyde oxidase selectivity and metabolic reactions. *J Med Chem* 2018;**61**:360–71.
20. Zhao J, Cui R, Wang L, Chen Y, Fu Z, Ding X, et al. Revisiting aldehyde oxidase mediated metabolism in drug-like molecules: an improved computational model. *J Med Chem* 2020;**63**:6523–37.
21. Montefiori M, Lyngholm-Kjærby C, Long A, Olsen L, Jørgensen FS. Fast methods for prediction of aldehyde oxidase-mediated site-of-metabolism. *Comput Struct Biotec* 2019;**17**:345–51.
22. Wieder O, Kohlbacher S, Kuenemann M, Garon A, Ducrot P, Seidel T, et al. A compact review of molecular property prediction with graph neural networks. *Drug Discov Today Technol* 2020;**37**:1–12.
23. Wu Z, Pan S, Chen F, Long G, Zhang C, Philip SY. A comprehensive survey on graph neural networks. *IEEE T Neur Net Lear* 2020;**32**:4–24.
24. Zhou J, Cui G, Hu S, Zhang Z, Yang C, Liu Z, et al. Graph neural networks: a review of methods and applications. *AI open* 2020;**1**:57–81.
25. Tian S, Djoumbou-Feunang Y, Greiner R, Wishart DS. CypReact: a software tool for *in silico* reactant prediction for human cytochrome P450 enzymes. *J Chem Inf Model* 2018;**58**:1282–91.
26. Lewis DF, Jacobs MN, Dickins M. Compound lipophilicity for substrate binding to human P450s in drug metabolism. *Drug Discov Today* 2004;**9**:530–7.
27. Young RJ, Green DV, Luscombe CN, Hill AP. Getting physical in drug discovery II: the impact of chromatographic hydrophobicity measurements and aromaticity. *Drug Discov Today* 2011;**16**:822–30.
28. Ferreira P, Cerqueira NMFSA, Fernandes PA, Romao MJ, Ramos MJ. Catalytic mechanism of human aldehyde oxidase. *ACS Catal* 2020;**10**:9276–86.

29. Xiong Z, Wang D, Liu X, Zhong F, Wan X, Li X, et al. Pushing the boundaries of molecular representation for drug discovery with the graph attention mechanism. *J Med Chem* 2019;**63**:8749−60.
30. Wang NN, Wang XG, Xiong GL, Yang ZY, Lu AP, Chen X, et al. Machine learning to predict metabolic drug interactions related to cytochrome P450 isozymes. *J Cheminf* 2022;**14**:23.
31. Rücker G, Schumacher M. Summary ROC curve based on a weighted Youden index for selecting an optimal cutpoint in meta-analysis of diagnostic accuracy. *Stat Med* 2010;**29**:3069−78.
32. Jia H, Dai G, Weng J, Zhang Z, Wang Q, Zhou F, et al. Discovery of (*S*)-1-(1-(imidazo[1,2-*a*]pyridin-6-yl)ethyl)-6-(1-methyl-1*H*-pyrazol-4-yl)-1*H*-[1,2,3]triazolo[4,5-*b*]pyrazine (Volitinib) as a highly potent and selective mesenchymal−epithelial transition factor (c-Met) inhibitor in clinical development. *J Med Chem* 2014;**57**:7577−89.
33. Gordon CP, Raynaud C, Andersen RA, Copéret C, Eisenstein O. Carbon-13 NMR chemical shift: a descriptor for electronic structure and reactivity of organometallic compounds. *Accounts Chem Res* 2019;**52**:2278−89.
34. Gordon CP, Lätsch L, Coperet C. Nuclear magnetic resonance: a spectroscopic probe to understand the electronic structure and reactivity of molecules and materials. *J Phys Chem Lett* 2021;**12**:2072−85.
35. Santos R, Ursu O, Gaulton A, Bento AP, Donadi RS, Bologa CG, et al. A comprehensive map of molecular drug targets. *Nat Rev Drug Discov* 2017;**16**:19−34.
36. Ayala-Aguilera CC, Valero T, Lorente-Macías Á, Baillache DJ, Croke S, Unciti-Broceta A. Small molecule kinase inhibitor drugs (1995−2021): medical indication, pharmacology, and synthesis. *J Med Chem* 2021;**65**:1047−131.
37. Ferguson FM, Gray NS. Kinase inhibitors: the road ahead. *Nat Rev Drug Discov* 2018;**17**:353−77.
38. Mukherjee P, Bentzien J, Bosanac T, Mao W, Burke M, Muegge I. Kinase crystal miner: a powerful approach to repurposing 3D hinge binding fragments and its application to finding novel bruton tyrosine kinase inhibitors. *J Chem Inf Model* 2017;**59**:2152−60.
39. Gilson MK, Tiqing L, Michael B, George N, Linda H, Jenny C. BindingDB in 2015: a public database for medicinal chemistry, computational chemistry and systems pharmacology. *Nucleic Acids Res* 2016;**44**:D1045−53.
40. Zhou ZH. A brief introduction to weakly supervised learning. *Natl Sci Rev* 2018;**5**:44−53.
41. Xiong J, Li Z, Wang G, Fu Z, Zhong F, Xu T, et al. Multi-instance learning of graph neural networks for aqueous p*K*a prediction. *Bioinformatics* 2022;**38**:792−8.
42. Wu J, Wan Y, Wu Z, Zhang S, Cao D, Hsieh CY, et al. MF-SuP-p*K*a: multi-fidelity modeling with subgraph pooling mechanism for p*K*a prediction. *Acta Pharm Sin B* 2023;**13**:2572−84.
43. Kang S, Kwon Y, Lee D, Choi YS. Predictive modeling of NMR chemical shifts without using atomic-level annotations. *J Chem Inf Model* 2020;**60**:3765−9.
44. Li M, Zhou J, Hu J, Fan W, Zhang Y, Gu Y, et al. DGL-LifeSci: an open-source toolkit for deep learning on graphs in life science. *ACS Omega* 2021;**6**:27233−8.